

# Band Symmetries and Singularities in Twisted Multilayer Graphene

E. J. Mele\*

*Department of Physics and Astronomy University of Pennsylvania Philadelphia PA 19104*

(Dated: March 1, 2022)

The electronic spectra of rotationally faulted graphene bilayers are calculated using a continuum formulation for small fault angles that identifies two distinct electronic states of the coupled system. The low energy spectra of one state features a Fermi velocity reduction which ultimately leads to pairwise annihilation and regeneration of its low energy Dirac nodes. The physics in the complementary state is controlled by pseudospin selection rules that prevent a Fermi velocity renormalization and produce second generation symmetry-protected Dirac singularities in the spectrum. These results are compared with previous theoretical analyses and with experimental data.

PACS numbers: 73.22.Pr, 77.55.Px, 73.20.-r

The variation of the electronic properties of few layer graphenes (FLG's) with their layer stacking is receiving increasing attention. FLG's represent a family of materials that bridge the pseudo relativistic properties of single layer graphene with the more conventional semimetallic behavior of bulk graphite. The atomic registry of neighboring layers and stacking sequence are structural parameters that determine their electronic properties<sup>1-5</sup>. In twisted FLG's where the crystallographic axes of neighboring layers are misaligned by a rotation angle  $\theta \neq n\pi/3$  the interlayer interactions produce remarkably rich physics that is being actively studied<sup>6-22</sup>.

This paper presents a continuum theory of the low energy electronic physics in twisted bilayer graphenes for small rotation angles, as illustrated in Fig. 1. Our approach reveals the existence of *two distinct* electronic states in this system that present quite different electronic properties. The behavior of one state is identified with the situation described by a frequently adopted continuum formulation of this problem<sup>8,16</sup>: the interlayer coupling renormalizes the Fermi velocities of the individual layers and hybridizes their Dirac cones in the spectral region where they merge. In the complementary state we find that the Fermi velocity renormalization is nearly completely prevented by a pseudospin selection rule and the interlayer hybridization inherits a novel momentum space geometry producing a set of *second generation* Dirac singularities. The behavior in this latter family agrees well with properties experimentally observed for rotationally faulted FLG's thermally grown on SiC (000 $\bar{1}$ )<sup>9,11,15</sup> suggesting that this physics is realized in this form of FLG. We briefly discuss the relation of our new results to prior theoretical and to experimental studies of these systems.

The physics described below is identified by consideration of the effects of the *lattice symmetry* on the low energy electronic physics. We show that the geometrical structure of the low spectrum is determined by a symmetry-allowed threefold anisotropy in the interlayer coupling amplitudes which, though absent from conventional two-center tight binding models, occur in empirical models of interlayer coupling in graphite. We find that

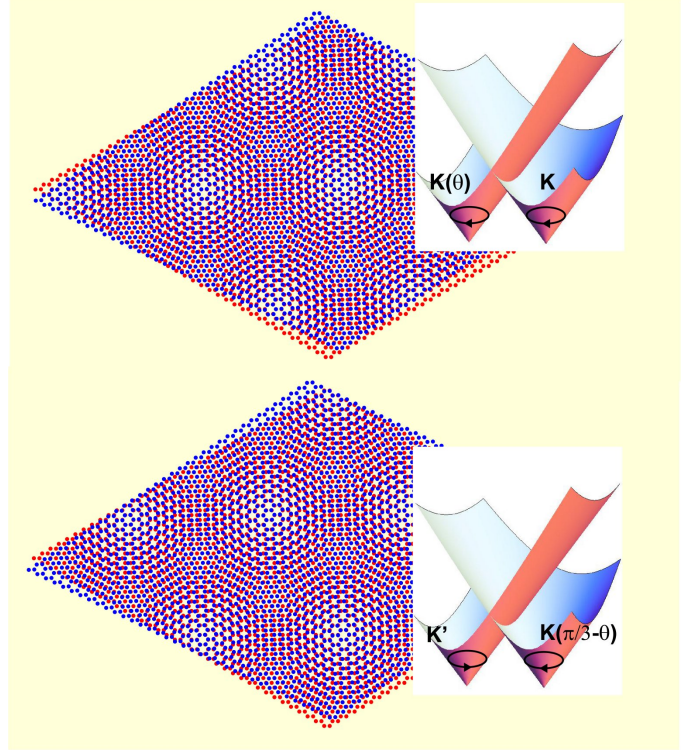


FIG. 1: Lattice structures of two twisted graphene bilayers rotated away from AA stacking by angles  $\theta = 3.89^\circ$  (top) and  $\theta = 56.11^\circ$  (bottom). The insets show schematically the dispersions of two nearby Dirac cones in these structures in the absence of their interlayer coupling.

the *sign* of this anisotropy distinguishes two quite different electronic states of this system.

The coupling between the two sublattices in the two layers can be represented by a (position dependent)  $2 \times 2$  matrix operator  $\hat{T}_{12}(\vec{r})$ . As shown in Figure 2, for small angle faults the registry between layers in the unit cell evolves smoothly from regions locally characterized by AB (region  $\alpha$ ), BA ( $\beta$ ) and AA ( $\gamma$ ). The smoothest possible supercell-periodic matrix-valued expression for

Coefficient	Parameterization	I	II
$t_G$	$(\gamma_1 - \gamma_3)/9$	43.3	8.3
$c_{aa}$	$\gamma_4 + (\gamma_1 - \gamma_3)/3$	130.0	69.0
$c_{ab}$	$(\gamma_1 + 2\gamma_3)/3$	130.0	340.0

TABLE I: Fourier coefficients (meV units) for the interlayer hopping operator Eqn. 2, fitted to the Slonczewski Weiss McClure parameterization for Bernal stacked layers. Model I:  $\gamma_1 = 390$  meV,  $\gamma_3 = \gamma_4 = 0$ . Model II:  $\gamma_1 = 390$  meV,  $\gamma_3 = 315$  meV and  $\gamma_4 = 44$  meV.

$\hat{T}(\vec{r})$  is given by the expansion

$$\hat{T}_{12}(\vec{r}) = \hat{t}_0 + \sum_{n=1}^6 e^{i\vec{G}_n \cdot \vec{r}} \hat{t}_n \quad (1)$$

with constant matrix coefficients  $\hat{t}_n$  and where  $\vec{G}_n$  are the six elements of the first star of reciprocal lattice vectors dual to the superlattice translations  $\vec{T}_1$  and  $\vec{T}_2$ . The matrix coefficients  $\hat{t}_n$  ( $n = 1, 6$ ) can be determined from the couplings in the locally registered regions; for example in the geometry of Figure 2 the even elements of the first star have coefficients

$$\hat{t}_{n \text{ even}} = t_G \begin{pmatrix} e^{-i\vec{G}_n \cdot \vec{r}_\gamma} & e^{-i\vec{G}_n \cdot \vec{r}_\alpha} \\ e^{-i\vec{G}_n \cdot \vec{r}_\beta} & e^{-i\vec{G}_n \cdot \vec{r}_\gamma} \end{pmatrix} = t_G \begin{pmatrix} z & 1 \\ z^* & z \end{pmatrix} \quad (2)$$

where  $z = e^{2\pi i/3}$  and the coefficients for the odd elements are  $t_{n \text{ odd}} = t_{n \text{ even}}^*$ . The constant matrix has the form

$$\hat{t}_0 = \begin{pmatrix} c_{aa} & c_{ab} \\ c_{ba} & c_{bb} \end{pmatrix} \quad (3)$$

with real coefficients satisfying  $c_{aa} = c_{bb}$  and  $c_{ab} = c_{ba}$ . The interlayer operator of Eqns. (2) and (3) is thus parameterized by three real constants  $t_G$ ,  $c_{aa}$  and  $c_{ab}$ . We choose these coefficients so that the interlayer matrix  $\hat{T}(\vec{r}_\alpha)$  matches the Slonczewski-Weiss-McClure (SWMcC) interlayer parameters  $\gamma_1$ ,  $\gamma_3$  and  $\gamma_4$  for Bernal stacked graphite shown in the inset of Figure 2<sup>24</sup> with the results in Table I. We note that the  $\gamma_3$  parameter (hopping between unaligned sublattices in the two layers) is comparable to  $\gamma_1$  and that the  $\gamma_4$  parameter (hopping between aligned and unaligned sublattice sites) is relatively weak.

The conventional continuum description of twisted bilayer graphene<sup>8,16</sup> can be derived from the constant matrix  $\hat{t}_0$ . The low energy Hamiltonian is a long wavelength expansion around the zone corner points in each layer; in this Dirac basis the matrix elements in Eqn. 1 acquire the phases  $\exp(i(\vec{G}' \cdot \vec{r}'_i - \vec{G} \cdot \vec{r}_j))$  where  $\vec{G}$  ( $\vec{G}'$ ) are reciprocal lattice vectors in the two separate layers and  $\vec{r}_j$  ( $\vec{r}'_i$ ) are sublattice positions. Boosts by a triad of  $(\vec{G}, \vec{G}')$  pairs translate the Hamiltonian to three pairs of zone corner points that are separated by  $\Delta\vec{K}$  and its  $\pm 2\pi/3$ -rotated counterparts. This generates three possible constant coupling matrices indexed by the momentum differences  $\Delta\vec{K}_i$ . With a conventional choice of origin<sup>8,16</sup>

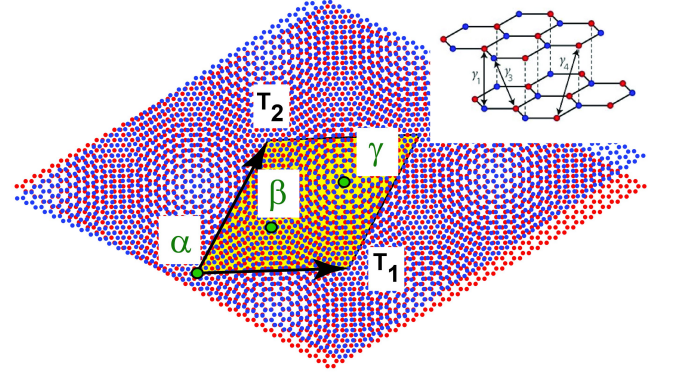


FIG. 2: Lattice structure for a segment of twisted bilayer at rotation angle  $3.89^\circ$ , with superlattice translation vectors  $T_1$  and  $T_2$ . The points labelled  $\alpha$ ,  $\beta$  and  $\gamma$  are high symmetry points in the unit cell. The inset<sup>23</sup> illustrates three hopping processes in the interlayer Hamiltonian.

where the  $A$  sublattice site of one layer is aligned with the  $B$  sublattice of the other, the matrices are

$$\begin{aligned} \hat{T}_1 &= \begin{pmatrix} 1 & 0 \\ 0 & 1 \end{pmatrix} \hat{t}_0 \begin{pmatrix} 1 & 0 \\ 0 & 1 \end{pmatrix} = \begin{pmatrix} c_{aa} & c_{ab} \\ c_{ba} & c_{bb} \end{pmatrix} \\ \hat{T}_2 &= \begin{pmatrix} 1 & 0 \\ 0 & z \end{pmatrix} \hat{t}_0 \begin{pmatrix} z & 0 \\ 0 & 1 \end{pmatrix} = \begin{pmatrix} z c_{aa} & c_{ab} \\ z^* c_{ba} & z c_{bb} \end{pmatrix} \\ \hat{T}_3 &= \begin{pmatrix} 1 & 0 \\ 0 & z^* \end{pmatrix} \hat{t}_0 \begin{pmatrix} z^* & 0 \\ 0 & 1 \end{pmatrix} = \begin{pmatrix} z^* c_{aa} & c_{ab} \\ z c_{ba} & z^* c_{bb} \end{pmatrix} \end{aligned} \quad (4)$$

In one of these valleys the Hamiltonian for the coupled bilayer with a momentum offset  $\Delta\vec{K}$  is

$$H = \begin{pmatrix} \hbar v_F \sigma \cdot (-i\nabla) & \hat{T}_1^\dagger \\ \hat{T}_1 & \hbar v_F \sigma_\theta \cdot (-i\nabla - \Delta\vec{K}) \end{pmatrix} \quad (5)$$

where  $\sigma_\theta$  are Pauli matrices resolved along the axes of the  $\theta$ -rotated layer. The problem can be written dimensionless form by scaling all momenta by the offset  $|\Delta\vec{K}|$  and energies by  $E_\theta = \hbar v_F |\Delta\vec{K}|$ . The scaled coupling coefficients are  $\tilde{c} = c/E_\theta = 3ac/(8\pi\hbar v_F \sin(\theta/2))$  (where  $a$  is the single layer graphene lattice constant) which increase with decreasing rotation angle.

Model I (Table I) is an isotropic interlayer model with  $\gamma_3 = \gamma_4 = 0$ . For an isotropic coupling model  $c_{aa} = c_{bb} = w$  and the interlayer matrices are

$$\hat{T}_1 = w \begin{pmatrix} 1 & 1 \\ 1 & 1 \end{pmatrix}; \hat{T}_2 = w \begin{pmatrix} z & 1 \\ z^* & z \end{pmatrix}; \hat{T}_3 = w \begin{pmatrix} z^* & 1 \\ z & z^* \end{pmatrix} \quad (6)$$

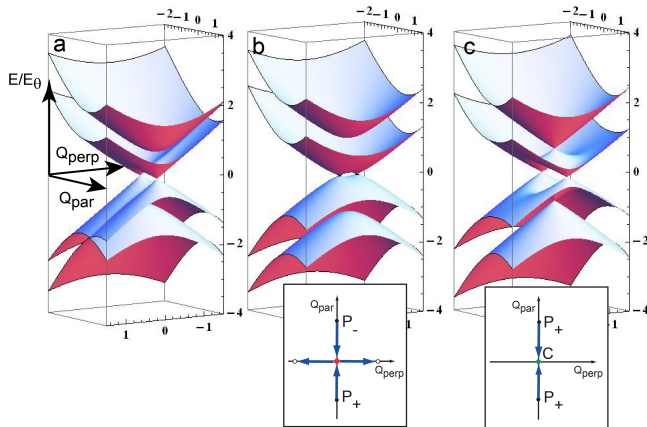


FIG. 3: Electronic spectra for twisted bilayers using the interaction parameters (a):  $\hat{t}_0 = \tilde{c}(\mathbf{I} + \sigma_x)$ ,  $\tilde{c} = 0.21$ , (b):  $\hat{t}_0 = \tilde{c}\sigma_x$ ,  $\tilde{c} = 0.55$  and (c):  $\hat{t}_0 = \tilde{c}\mathbf{I}$ ,  $\tilde{c} = 0.55$ .  $Q_{\text{par}}$  and  $Q_{\text{perp}}$  are momenta in units of the offset  $|\Delta\vec{K}|$  and the ordinate is the scaled energy  $E/E_\theta = E/(\hbar v_F \Delta K)$ . In (b) Dirac cones with opposite helicity are coupled, in (c) Dirac cones with the same helicity are coupled. The insets give the locations of singular points in the spectra describing the annihilation and regeneration of Dirac nodes (red diamond) in the compensated case (b) and the appearance of a singular point of degeneracy (C) for the uncompensated case (c). The point C is a second generation Dirac point singularity in the coupled spectrum.

with  $w = 130$  meV. The form of these matrices and their prefactor agree with the estimates ( $w \approx 110$  meV) obtained from tight binding calculations<sup>8,16</sup>. Our construction shows that these terms project the  $q = 0$  term of the interlayer potential into the Dirac  $K$ -point (pseudospin) basis thereby coupling the electronic states in the two layers with identical crystal momenta. Since only the  $q = 0$  term in the coupling is retained it does not depend on a relative lateral translation of the two layers, in agreement with earlier work<sup>16</sup> and physically reasonable since for small twist angle a rigid layer translation produces insignificant changes to the Moire superlattice. Thus Model I reproduces the existing continuum theoretic phenomenology of the coupled system, and the calculation leading to Eqn. 6 provides an alternate (and compact) derivation of the effective Hamiltonian used in these earlier studies<sup>8,16</sup>. The left panel of Fig. 3 shows the bilayer spectra computed in this model which shows the expected ( $\theta$ -dependent) reduction of the Dirac cone velocities and a hybridization of the two branches in the spectral region where they merge.

We now consider a refinement of the interlayer coupling matrices using the parameterization of Model II. The salient properties of the SWMcC parameterization are the introduction of the interlayer amplitudes  $\gamma_3$  and

$\gamma_4$  with  $\gamma_3$  comparable to  $\gamma_1$  and  $\gamma_4$  significantly smaller. Note that  $\gamma_3$  and  $\gamma_4$  represent interlayer hopping processes at the same range but in different directions with respect to the layer crystallographic axes. The asymmetry between  $\gamma_3$  and  $\gamma_4$  thus reflects an intrinsic threefold lattice anisotropy in the interlayer amplitudes which, though symmetry-allowed, does not occur in the isotropic two center tight binding approximation. Significantly, these additional terms *break the symmetry* between the pseudospin-diagonal and off diagonal terms in  $\hat{t}_0$  (Table I) so that the coupling matrix is dominated by its off diagonal amplitudes. An instructive limit considers  $\hat{t}_0 \propto \sigma_x$  for which the Fig. 3(b) shows the spectrum calculated for a  $\theta = 3.89^\circ$  rotation away from Bernal stacking. Here the two Dirac cones have *merged* at low energy producing two composite low energy singular points. Note that the linear low energy dispersion is replaced by an approximately quadratic form near the center of symmetry of these spectra and that the momentum offset between the singular points in the spectrum is along the  $Q_{\text{perp}}$  axis, i.e.  $\pi/2$ -rotated with respect to the original Dirac cone offset  $\Delta\vec{K}$ .

These spectral changes reflect the proximity to a critical point that occurs at  $\tilde{c} = 1/2$  in this theory. This can be understood by considering a single layer sublattice exchange operation implemented by the gauge transformation

$$\begin{aligned} \tilde{H} &= \begin{pmatrix} \mathbf{I} & 0 \\ 0 & \hat{\sigma}_x \end{pmatrix} \begin{pmatrix} \hat{H}_K(\vec{q}) & \tilde{c}\hat{\sigma}_x \\ \tilde{c}\hat{\sigma}_x & \hat{H}_K(\vec{q} - \Delta\vec{K}) \end{pmatrix} \begin{pmatrix} \mathbf{I} & 0 \\ 0 & \hat{\sigma}_x \end{pmatrix} \\ &= \begin{pmatrix} \hat{H}_K(\vec{q}) & \tilde{c}\mathbf{I} \\ \tilde{c}\mathbf{I} & \hat{\sigma}_x \cdot \hat{H}_K(\vec{q} - \Delta\vec{K}) \cdot \hat{\sigma}_x \end{pmatrix} \end{aligned} \quad (7)$$

demonstrating that this system has a scalar coupling Dirac cones with compensating helicities (Berry's phase  $\pm\pi$ ). Increasing the control parameter  $\tilde{c}$  (by decreasing  $\theta$ ) draws the nodes together until they become coincident at a critical coupling strength  $\tilde{c} = 1/2$  and annihilate (Fig. 3b inset). For  $\tilde{c} > 1/2$  new singularities emerge at  $E = 0$  separated by  $\Delta\vec{Q}$  directed *perpendicular* to the original offset  $\Delta\vec{K}$ . Using the parameters listed in Table II,  $\tilde{c}(\theta = 3.89^\circ) = 0.55$ , i.e. just on the strong coupling side of this transition. The residual curvature in the low energy spectrum and the associated reorientation of  $\Delta\vec{Q}$  are both clearly evident in Fig. 3b. It is noteworthy that the momentum separation between the zero energy contact points is generally *not* determined purely geometrically by the rotation angle as is generally assumed, but instead is modified by the interlayer coupling. This occurs because the interactions between layers produces an effective gauge field seen within each layer that shifts the momentum of its zero energy states. The  $\pi/2$  rotation of the momentum offset that bridges the contact points on the strong coupling side of the transition is a striking consequence of this gauge coupling.

Reversing the *sign* of the threefold anisotropy in the interlayer matrix  $\hat{t}_0$  produces a distinct electronic state.

The complementary behavior is understood by considering the limit  $\hat{t}_0 \propto \mathbf{I}$  which describes the coupling of Dirac cones with the *same* helicity, preventing annihilation of the Dirac nodes and leading to a qualitatively different geometry in the bilayer spectrum (Fig. 3c). The dispersing bands from the uncoupled cones are degenerate everywhere along the line that bisects  $\Delta\vec{K}$ . However, along the line that connects the Dirac nodes the pseudospins are *orthogonal* and the interlayer coupling is symmetry-forbidden, turning on linearly as a function of the transverse momentum  $Q_{\text{perp}}$ . Thus the coupled system retains a twofold point degeneracy midway between the displaced Dirac nodes<sup>25</sup>. The cancellation of the interlayer coupling at this critical point is the bilayer analog of the “absence of backscattering” due to the  $\pi$  Berry’s phase in single layer graphene. In the vicinity of this critical point interlayer coupling is allowed and proportional to the transverse momentum. Thus this system exhibits *second generation Dirac singularities* in its coupled layer spectrum as shown in Fig. 3c: hybridization of the two layers is symmetry forbidden at a discrete critical crossing point. We refer to this complementary state as the uncompensated bilayer state.

The relative helicity of the two Dirac cones also controls the renormalization of their Fermi velocities, further distinguishing these two states. For Dirac cones of opposite helicities, perturbation theory on the Hamiltonian in Eqn. 7 for small  $\tilde{c}$  modifies the velocity operators

$$\begin{aligned}\hat{v}_+ &= v_F\sigma_+ \rightarrow v_F(1 - \tilde{c}^2)\sigma_+ \\ \hat{v}_- &= v_F\sigma_- \rightarrow v_F(1 - \tilde{c}^2)\sigma_-\end{aligned}\quad (8)$$

which symmetrically reduces both  $v_x$  and  $v_y$ ; summation over the triad of offset momenta  $\Delta\vec{K}_i$  yields the renormalized velocity  $v_F^* = v_F(1 - 9\tilde{c}^2)$  exactly as found in earlier work<sup>8,16</sup>. By contrast for coupling between nearby cones of the same helicity perturbation theory yields

$$\begin{aligned}\hat{v}_+ &= v_F\sigma_+ \rightarrow v_F(\sigma_+ - \tilde{c}^2\sigma_-) \\ \hat{v}_- &= v_F\sigma_- \rightarrow v_F(\sigma_- - \tilde{c}^2\sigma_+)\end{aligned}\quad (9)$$

so that in this class the corrections to the velocity are weaker,  $\propto \tilde{c}^4$ . Moreover they have a *twofold*  $\cos(2\phi)$  anisotropy so they vanish by symmetry after summing over the threefold symmetric triad of  $\Delta\vec{K}_i$ . Thus the Fermi velocity is unchanged by the interlayer coupling in this class of bilayers. Physically this can be understood by observing that the bands dispersing through the Dirac nodes are connected smoothly to the second generation points of degeneracy at  $\Delta\vec{K}/2$ .

The distinction between the compensated and uncompensated states in the small angle limit reflects a lattice-scale property that determines the matrix structure of the long wavelength coupling in Eqn. 1. This should be distinguished from the different mechanism by which sublattice exchange symmetry determines the direct coupling between the Dirac nodes<sup>14</sup>. The latter requires *finite momentum* umklapp interlayer hopping processes

which, though significant for low order rational commensurate rotations, are negligible in the small angle limit considered here. For example, note that sublattice exchange “even” and “odd” commensurations are related by a rigid sublattice translation of one layer at a *fixed* rotation angle. In the small angle regime this translation simply permutes regions of the bilayer that are locally in *AB*, *BA* and *AA* registry as shown in Fig. 1, but it does not change  $\hat{t}_0$  which determines the spectrum. Thus sublattice exchange “even” and “odd” structures become indistinguishable in the small angle limit. Note also that bilayers at rotation angles  $\theta$  and  $\theta = \pi/3 - \theta$  are commensuration pairs that can be distinguished by their sublattice exchange parity<sup>14</sup>. Even and odd parity commensurations are, respectively, inflated generalizations of the primitive *AA* and *AB* stacked bilayers. This symmetry ultimately determines the valley structure of the interlayer amplitudes that directly couple the Dirac nodes of neighboring layers. This interlayer umklapp coupling derives from the finite momentum terms in the interlayer Hamiltonian in contrast to the  $q = 0$  terms that control the physics for small angle rotations.

The spectra for these two classes are ultimately determined by the pseudospin asymmetry in  $\hat{t}_0$ . The conventional SWMcC model selects the class that couples cones with compensating helicities. In this model the spectral transition illustrated in Figure 3 occurs for rotation angles near  $4^\circ$ , i.e. in a range that is frequently studied experimentally<sup>17,18</sup>. The physics of the uncompensated class occurs for  $c_{aa} > c_{ab}$  which requires  $\gamma_4 > \gamma_3$ . Although this is excluded by the conventional SWMcC parameterization it is important to note that this parameterization is designed to fit data for Bernal stacking, and it likely does not properly represent the matrix structure of the coupling in *AA* registered regions. In particular using the parameterization of Table I, the spatial dependence of Eqn. 1 shows that strong interlayer coupling in *AA* stacked regions requires  $\gamma_4 > \gamma_3$ . Microscopically this originates from interlayer tunneling processes along the edges of eclipsed hexagons in the aligned *AA* structure, a motif which does not appear at all for Bernal stacking. In the spirit of the SWMcC theory it is therefore appropriate to retain  $\gamma_3$  and  $\gamma_4$  as parameters which can be determined from the experimentally observed properties of twisted graphenes.

In fact the phenomenology of the uncompensated class provides a striking explanation for many of the puzzling observed spectral properties for rotationally faulted graphenes thermally grown on  $\text{SiC}(000\bar{1})$ <sup>11,12,15</sup>. Landau level spectroscopy shows a negligible renormalization of the Fermi velocity in these structures<sup>12</sup> and furthermore angle resolved photoemission finds no evidence for a hybridization-induced avoided crossing of the intersecting Dirac cones, despite a careful search<sup>15</sup>. This is completely consistent with the existence of a node in the interlayer coupling at the midpoint between offset Dirac cones characteristic of the uncompensated class. This assignment can be confirmed definitively by measurements

of the quasiparticle dispersion along an azimuth passing through the midpoint between the displaced Dirac cones, but *perpendicular* to  $\Delta\vec{K}$ ; these should show a band splitting linear in the transverse momentum around the point of degeneracy. Alternatively, if these bilayers exist in the compensated class, photoemission should be able to detect the annihilation and re-emergence of their singular contact points along with the band curvature in their spectra in the crossover regime as illustrated in Fig. 3(b).

By contrast, experiments on rotationally faulted CVD-grown graphenes have observed phenomena that have been associated with the spectral properties of the compensated class<sup>18,20</sup>. Features due to the van Hove singularities arising from an the avoided crossing of hybridized Dirac cones<sup>18</sup> and a  $\theta$ -dependent low energy velocity renormalization have both been reported<sup>20</sup>. These features are at least qualitatively consistent with the predicted behavior of the compensated class and have been analyzed within a theoretical model representative of this class<sup>8</sup>. We note that these measurements study samples at small rotation angle where the proximity to the merger of the Dirac singularities (Fig. 3) should be manifest in these data though their effects have not yet been considered in the analysis. It is interesting that these samples exhibit a large periodic height modulation  $\approx 1\text{\AA}$  in the superlattice unit cell peaked in the *AA*-registered zones<sup>26</sup>. It is tempting to speculate that these CVD samples are grown as rippled structures that partially delaminate in these regions thereby locally weakening their contribution to the  $q = 0$  coupling coefficients. In this sce-

nario the strongly coupled regions would maintain Bernal registry as described by the conventional SWMcC parameterization and identify these samples as members of the compensated bilayer family.

The distinction between the two complementary states is controlled by an important three-fold anisotropy in the interlayer tunneling amplitudes. This physics is not captured by an isotropic two-center tight binding theory, which inevitably leads one to the coupling model in Eqn. 6 which happens to occur at a crossover between two rather different electronic models for the system. The effects of the threefold anisotropy are accessible in density functional calculations of these structures, but for practical reasons these have been restricted to short period superlattices which do not address the small angle regime where the continuum theory is most appropriate. For short period commensurate structures, the Fermi velocities found in these calculations are consistent with the values for single layer graphene. This could arise from the small value of  $\tilde{c}$  in the large angle regime, the intrinsic behavior of the uncompensated class or an interlayer mass term which is important for short period superlattices<sup>14</sup>.

I thank P. First, C. Kane, M. Kindermann, S. Zaheer and F. Zhang for their comments on the manuscript E. Andrei for communication of unpublished data. This work was supported by the Department of Energy, Office of Basic Energy Sciences under contract DE-FG02-ER45118.

---

\* Electronic address: mele@physics.upenn.edu

<sup>1</sup> E. McCann and V.I. Fal'ko, Phys. Rev. Lett **96**, 086805 (2006).  
<sup>2</sup> T. Ohta *et al.*, Science **313**, 951 (2006).  
<sup>3</sup> F. Guinea, A.H. Castro Neto, and N.M.R. Perez, Phys. Rev. B **73**, 245426 (2006).  
<sup>4</sup> H. Min, A.H. MacDonald, Phys. Rev. B **77**, 155416 (2008).  
<sup>5</sup> M. Koshino and E. McCann, Phys. Rev. B **80**, 165409 (2009).  
<sup>6</sup> C. Berger *et al.*, Science **312**, 1191 (2006).  
<sup>7</sup> S. Latil *et al.*, Phys. Rev. B **76**, 201402(R) (2007).  
<sup>8</sup> J.M.B. Lopes dos Santos, N.M.R. Peres, A.H. Castro Neto, Phys. Rev. Lett. **99**, 256802 (2007).  
<sup>9</sup> J. Hass *et al.*, Phys. Rev. Lett. **100**, 125504 (2008).  
<sup>10</sup> S. Shallcross, S. Sharma and O.A. Pankratov, Phys. Rev. Lett.**101**, 056803 (2008).  
<sup>11</sup> M. Sprinkle *et al.* Phys. Rev. Lett. **103**, 226803 (2009).  
<sup>12</sup> D.M. Miller *et al.* Science **324**, 9242 (2009).  
<sup>13</sup> G. T. de Laissardière *et al.* Nano Lett. **10**, 804 (2010).  
<sup>14</sup> E. J. Mele, Physical Review B **81**, 161405 (2010).

<sup>15</sup> J. Hicks *et al.*, Phys. Rev. B **83**, 205403 (2011).

<sup>16</sup> R.Bistritzer and A.H. MacDonald, Proc. Nat. Acad. Sci. **108**,12233 (2011).  
<sup>17</sup> G. Li, A. Luican and E.Y. Andrei, Phys. Rev. Lett. **102**, 176804 (2009).  
<sup>18</sup> G. Li *et al.* Nature Physics **6**, 109 (2010).  
<sup>19</sup> M. Kindermann and P.N. First, Physical Review B **83**, 045425 (2010).  
<sup>20</sup> A. Luican *et al.* Phys. Rev. Lett. **106**, 126802 (2011).  
<sup>21</sup> R. de Gail *et al.*, Phys. Rev. B **84**, 045436 (2011).  
<sup>22</sup> M-Y Choi, H-Y Hyun and Y. Kim, Phys. Rev. B **84**, 195437 (2011).  
<sup>23</sup> M. Freitag Nature Physics **7**,596 (2011).  
<sup>24</sup> M.S. Dresselhaus and G. Dresselhaus, Advances in Physics **51**, 1 (2002) (p. 69).  
<sup>25</sup> Because of the rotation of  $\sigma_\theta$  in Eqn. 6 this point degeneracy is slightly shifted along the line that bisects  $\Delta\vec{K}$ . This does not significantly change the physics.  
<sup>26</sup> E.Y. Andrei (unpublished).